



**HAL**  
open science

# Development of an Inverse Approach for the Characterization of In Vivo Mechanical Properties of the Lower Limb Muscles

Jean-Sébastien Affagard, Sabine Bensamoun, Pierre Feissel

► **To cite this version:**

Jean-Sébastien Affagard, Sabine Bensamoun, Pierre Feissel. Development of an Inverse Approach for the Characterization of In Vivo Mechanical Properties of the Lower Limb Muscles. *Journal of Biomechanical Engineering*, 2014, 136 (11), 10.1115/1.4028490 . hal-03809954

**HAL Id: hal-03809954**

**<https://hal.utc.fr/hal-03809954>**

Submitted on 12 Oct 2022

**HAL** is a multi-disciplinary open access archive for the deposit and dissemination of scientific research documents, whether they are published or not. The documents may come from teaching and research institutions in France or abroad, or from public or private research centers.

L'archive ouverte pluridisciplinaire **HAL**, est destinée au dépôt et à la diffusion de documents scientifiques de niveau recherche, publiés ou non, émanant des établissements d'enseignement et de recherche français ou étrangers, des laboratoires publics ou privés.

# Development of an inverse approach for the characterization of in vivo mechanical properties of the lower limb muscles

<sup>1,2</sup>Jean-Sébastien Affagard, PhD

<sup>1</sup>Sabine F. Bensamoun, Ph.D

<sup>2</sup>Pierre Feissel, Ph.D

<sup>1</sup>Université de Technologie de Compiègne, UMR CNRS 7338, BioMécanique et  
BioIngénierie, Compiègne, France

<sup>2</sup>Université de Technologie de Compiègne, UMR CNRS 7337, Laboratoire Roberval,  
Compiègne, France

Original article

Word count: 3965

## **Corresponding author**

Dr Sabine F. Bensamoun

Université de Technologie de Compiègne (UTC)  
Centre de recherches de Royallieu  
Laboratoire de BioMécanique et BioIngénierie, UMR CNRS 7338  
Rue Roger Couttolenc  
CS 60319  
60203 Compiègne  
France  
Tel: (33) 03 44 23 43 90  
Email: sabine.bensamoun@utc.fr

## ABSTRACT

The purpose of this study was to develop an inverse method, coupling imaging techniques with numerical methods, to identify the muscle mechanical behavior.

A Finite Element **Model** Updating (FEMU) was developed in three main interdependent steps. Firstly a 2D FE modeling, parameterized by a Neo-Hookean behavior ( $C_{10}$ ,  $D$ ), was developed from a segmented thigh muscle MRI (1.5T). Thus, a displacement field was simulated for different static loadings (contention, compression, indentation). Subsequently, the optimal mechanical test was determined from a sensitivity analysis. Secondly, ultrasound parameters (gain, dynamic and frequency) were optimized on the thigh muscles in order to apply the digital image correlation (DIC), allowing the measurement of an experimental displacement field. Thirdly, an inverse method was developed to identify the Neo-Hookean parameters ( $C_{10}$ ,  $D$ ), by performing a minimization of the distance between the simulated and measured displacement fields. To replace the experimental data and to quantify the identification error, a numerical example was developed.

The result of the sensitivity analysis showed that the compression test was more adapted to identify the Neo-Hookean parameters. Ultrasound images were recorded with a frequency, gain and dynamic of 9MHz, 34db, 42db, respectively. In addition, the experimental noise on displacement field measurement was estimated to 0.2 mm. The identification performed on the numerical example revealed a low error for the  $C_{10}$  ( $< 3\%$ ) and  $D$  ( $< 7\%$ ) parameters with the experimental noise.

This methodology could have an impact in the scientific and medical fields. A better knowledge of the muscle behavior will help to follow treatment and to ensure accurate medical procedures during the use of robotic devices.

## 1. INTRODUCTION

Several types of elastic garments have been developed to facilitate recovery, to increase performance or to prevent muscular lesions and pathologies. These elastic compressions mainly improve the backflow of blood to the heart. The influence of the compression was determined by hemodynamic or measurement of physiological parameters, during or after exercise, and its effect on the recovery or performances was analyzed with contradictory results [1]. A way to study the impact of the restraint is to use the muscle mechanical behavior as an indicator [2-4].

Recently, medical imaging was further developed as a clinical tool to assess the muscle mechanical behavior. Elastography techniques, based on ultrasound [5-6] or Magnetic Resonance Imaging [7-9], were used in clinical practice by applying a dynamic excitation. Subsequently, the assumption of infinitesimal strain theory provided the elastic and viscous parameters of the muscle [5, 8]. Medical imaging can be also used to identify the linear elastic properties from a static loading using similar assumptions [10-12]. However, in case of finite strain theory the muscle behavior will not be correctly represented.

A way to better describe these large strains was to characterize the nonlinear properties of the muscle, represented by an incompressible [13-14.] or a compressible [2-3, 15] hyperelastic behavior. Thus, tumors from breast tissue were discerned using the spatial distribution of the hyperelastic material properties [16, 17]. Indeed, B-mode ultrasound signal was correlated between several images [18, 19] in order to measure the displacement and strain fields. Other studies used Magnetic Resonance Imaging with quasi-static loading in order to identify the Neo-Hookean hyperelastic soft tissue behavior [2-3, 15]. Thus, the skin, the muscle and the

bone contours were obtained from MRI deformed muscle images, and then compared with the finite element simulation built from a 2D segmented MRI. Instead of using the contours, the MR tagging method was developed to measure the displacement and strain fields [20, 21]. Currently, only the relation between the force and the displacement was identified and not the muscle behavior.

The challenge of this work is to develop experimental and numerical tools allowing the identification of the hyperelastic heterogeneous mechanical behavior of muscle tissues. The experimental protocol was based on ultrasound image acquisitions which were coupled with Digital Image Correlation (DIC) to evaluate the displacement field. It must be noted that the DIC method was never applied from *in vivo* human soft tissue ultrasound acquisitions. Thus, the experimental issue was the optimization of the ultrasound parameters. In parallel, the first numerical issue was to determine the mechanical test in order to obtain the compressible hyperelastic parameters. The second numerical issue was to validate the present inverse method through the estimation of the identification error from a developed numerical example.

## 2. MATERIALS AND METHODS

### 2.1. Identification approach

The Finite Element Model Updating (FEMU) was decomposed in three main interdependent steps: the set-up of an experimental protocol (Fig. 1.C), the development of a finite element model (Fig. 1.A), and the development of an inverse method (Fig. 1.D).

#### 2.1.1. Experimental protocol

The set up was previously published by Affagard et al. [22] and is briefly described. A mechanical loading was applied on the thigh muscles (Fig. 2), and ultrasound images of uncompressed and compressed muscle were acquired on the lower third part of the thigh because this area was surrounded with less adipose tissue. Thus, the muscle tissues were more easily to strain. Scans were acquired with an ultrasound system (Logiq-E9, GE Healthcare, US) with a ML6-15 probe (GE Healthcare, US). The probe was positioned on the thigh transversal slice and fixed in order to avoid motion. Then, a Digital Image Correlation (DIC) was performed between these 2 images in order to obtain a measurement of the horizontal and vertical displacement fields [23, 24] which was the first input of the present identification process. The ultrasound images had to be acquired with a specific texture (high contrast and dynamic of the speckle) required by the DIC in order to perform the full-field measurement. The displacement field measurement was performed with the Correli\_Q4 software [25, 26]. The particularity of this software is to regularize the displacement field as a decomposition of shape functions.

### 2.1.2. Finite element model

The computational modeling ran on ABAQUS software [27] and was developed to obtain the muscle simulated displacement field. A 2D Finite Element (FE) model of the thigh was developed considering the plane strain assumption.

#### *2.1.2.1. Mesh generation*

The geometry of the thigh was obtained with a 1.5T MRI machine (GE, Signa HDx, Milwaukee, WI, USA) and a fast spin echo sequence (TR: 1800ms, TE: 7ms, FOV: 1518x3068, thickness: 3mm). Then, the slice of interest was segmented using Scan IP software (Simpleware, Exeter, UK) [28]. For the FE model, the bone was considered rigid due to its higher stiffness compared to its environmental soft tissues. The thigh geometry was divided in five regions corresponding to the adipose tissue and four muscles (quadriceps, ischio, gracilis and sartorius) (Fig. 1.A). The mesh was created using ABAQUS software. The mesh validation was performed by comparing the type (hybrid formulation and reduced integration) and the number of elements. Hybrid formulation allowed to avoid the hourglass effects. In addition, the integration was performed on 4 gauss points because the accuracy of the nodal displacement must be lower than the experimental noise ( $10^{-2}$  mm). Subsequently, the number of elements was tested (from 6000 to 26 000 nodes) using the fixed parameters (Table 1). The accuracy of the nodal displacement was lower than  $10^{-4}$  mm whatever the number of elements was. However, the number of elements was chosen to 25 392 in order to avoid the distortion during the identification process. Thus, the mesh was composed of 25392 CPE4H elements (4-node linear elements, hybrid with constant pressure), corresponding to 40776 nodes, and the integration was performed on 4 gauss points. Each tissue was assumed to be homogeneous. The skin and the blood vessels were not modelled. The skin was included in the adipose tissue area and the blood vessels were incorporated in the nearest soft tissue. It

was assumed that the incorporated tissues contributed to the average, in terms of elastic properties.

#### 2.1.2.2. Material constitutive law

In this study, the soft tissue mechanical behavior was assumed to be compressible hyperelastic, governed by the assumption of large strain theory. The compressibility was justified by a volume variation before and after the mechanical loading [2, 3].

A Neo-Hookean behavior ( $C_{10}$ ,  $D$ ) was chosen and the strain energy density function ( $W$ ) was written as:

$$W = C_{10}(\bar{I}_1 - 3) + \frac{1}{D}(J - 1)^2 \quad (1)$$

Where  $C_{10}$  and  $D$  are parameters describing the hyperelastic behavior,  $J = \det(\underline{\underline{F}})$ ,  $\bar{I}_1 = J^{-2/3} \cdot I_1$  and  $I_1 = Tr(\underline{\underline{F}}^T \cdot \underline{\underline{F}})$  with  $\underline{\underline{F}}$  the deformation gradient tensor and  $Tr$  the matrix trace.

The  $D$  parameter is the compressibility parameter and  $K = D/2$  is the bulk modulus.

The hyperelastic behavior of the entire model was driven by ten parameters:  $C_{10}^f$  and  $D^f$  for the adipose tissue,  $C_{10}^q$  and  $D^q$  for the quadriceps muscle,  $C_{10}^i$  and  $D^i$  for the ischio muscle,  $C_{10}^s$  and  $D^s$  for the sartorius muscle and  $C_{10}^g$  and  $D^g$  for the gracilis muscle. All these parameters are collected in a vector, denoted  $\theta$ .

#### 2.1.2.3. Quasi-static loading tests and boundary conditions

Different numerical static loadings (contention, compression, indentation) (Fig. 3) were simulated to evaluate the best test enabling an accurate and fast identification of all parameters ( $C_{10}$ ,  $D$ ). In order to characterize the adipose tissue and the four muscles, it was necessary to perform either four indentation tests or two compression loadings or one

contention test. Along the internal bone contour (femur), Dirichlet conditions, which fix all degrees of freedom, were imposed. Along the external contour, the boundary conditions which depend on the applied quasi-static loading were applied.

Concerning the contention test (Fig. 3.A), a Neumann condition equal to 20 mmHg pressure, corresponding to a classic containment pressure, was imposed. As for the indentation (Fig. 3.B) and the compression (Fig. 3.C) tests, a rigid body was added to simulate the loading with a force of 3N and 0.1N, respectively. These load levels were chosen so that the maximal stress was the same (Figs. 3.D-F).

### 2.1.3. Inverse method

To identify the ten material parameters ( $C_{10}$ ,  $D$ ), a cost function ( $J(\theta)$ ) based on the comparison of the measured and simulated displacement fields (Fig. 1.D) was defined as a quadratic discrepancy:

$$J(\theta) = 1/2 (\tilde{U} - \bar{U}(\theta))^T (\tilde{U} - \bar{U}(\theta)) \quad (2)$$

where  $\tilde{U}$  is the simulated displacement referring to the data from the numerical example mimicking the experiment and  $\bar{U}$  is the calculated displacement. The identification of  $\theta$  was performed through the minimization of the cost function in order to yield the best set of parameters in a least square manner. The minimization was carried out through a BFGS (Broyden–Fletcher–Goldfarb–Shanno) algorithm (MATLAB 2009).

## 2.2. Set up of the ultrasound parameters

To perform the DIC in optimal conditions, the ultrasound image speckle must have a high contrast and a high dynamic. Several preliminary adjustments were performed and only three interdependent parameters (frequency, gain and dynamic) were considered to have a significant influence on DIC result. The frequency, the gain and the dynamic have an impact on the signal/noise ratio, the pixel intensity and the contrast, respectively.

These ultrasound images were acquired on two male and two female sportive volunteers ( $30.5 \pm 3.5$  years old, BMI = 21.3) without venous and muscle pathologies. Three criteria were introduced in order to evaluate the image quality:

- a. To acquire the bone tissue in order to use it as a boundary condition for the FE modeling
- b. To obtain a large grey level distribution without any saturation
- c. To obtain the lowest displacement random error following the application of the DIC

The first criterion was related to the bone depth information. Due to the bone depth within the thigh, the ultrasound acquisitions were performed on the back side (biceps femoris) where it was possible to acquire bone and muscle on the same ultrasound image. Subsequently, the ultrasound acquisition frequency was decreased (13 MHz, 11 MHz, 9 MHz) until the information of bone depth area was sufficient for performing DIC whatever the thigh section of interest was with the highest spatial resolution (Fig. 4). During this tuning, the gain and the dynamic parameters were chosen in a medium range corresponding to 47 dB and 42 dB, respectively.

The second criterion was based on the grey histograms which are dependent of the image contrast influenced by the gain (G) parameter and the dynamic (Dyn) one. Both

parameters impact the pixel intensity. Indeed, in the mechanical field, the speckle is usually a random white and black distribution in order to perform the DIC [25]. In the present ultrasound thigh images, the black and white colors show up in the same area leading to saturation peak harmful for the DIC.

For instance, the couple (G: 30 dB, Dyn: 42 dB) provided a large repartition of the grey level histogram with a low saturation (black: 0 or white: 255 level) (Figs. 5.A,D). An increase of the gain (G: 37 dB) showed a shift of the grey level histogram (Figs. 5.B,E) while an increase of the dynamic (Dyn: 96 dB) revealed a narrow histogram (Figs. 5.C,F). In addition, the dynamic parameter has an effect on the contrast leading to an adjustment of the gain (G: 65 dB).

Subsequently, the gain and dynamic parameters were optimized based on the results of the grey level histogram. Several values of the dynamic, available in the Logiq-E9 ultrasound machine, were fixed (36 dB, 42 dB, 48 dB, 51 dB, 54 dB, 57 dB), and for each one, few gains (from 26 dB to 45 dB) were tested in order to define the optimal ones (Fig. 6).

From the optimal gain and dynamic parameters, the third criterion represented by the lowest displacement random error was quantified.

Thus, two ultrasound acquisitions realized with an interval of few seconds ( $\approx 3$  to 5 seconds) were acquired without compression in the quadriceps area (Fig. 2) for eight subjects. Then, the DIC was applied in order to measure the horizontal and vertical displacement fields. Subsequently, the standard deviation of the measured displacement fields was considered as an indicator of the random error since any loading was performed on the thigh, and it was assumed that the soft tissues were not deformed.

For each subject and each couple (gain/dynamic), the ultrasound acquisitions were repeated 13 times, corresponding to 12 DIC leading to 12 standard deviations.

Paired t-tests were performed in order to compare the standard deviations of the horizontal and vertical displacement fields between each couple. The statistical analysis was significant for  $P < 0.05$  using the software Statgraphics 5.0 (Sigma Plus, Maryland, USA).

### **2.3.Determination of the mechanical test from a sensitivity analysis**

To determine the optimal loading, a sensitivity ( $S$ ) analysis was performed on each mechanical test. The sensitivity of the finite element displacement field ( $U$ ) was carried out for each Neo-Hookean's parameter ( $\theta_k$ ) following the criteria proposed by Tarantola [29]:

$$S_{\theta_k} = \left\| \frac{\partial U}{\partial \theta_k} \right\| / \left\| U / \theta_k \right\|, \quad \forall k \in \{1, \dots, 10\} \quad (3)$$

where  $k$  represents each line number of the vector  $\theta$ .

The derivative was estimated from a finite difference approximation with a parameters step of  $5 \cdot 10^{-2} \%$  [30]. A higher sensitivity corresponds to a more influent material parameter on the displacement fields.

### **2.4.Numerical example**

The development of the numerical example (Fig. 1.B) had two aims. The first was to replace the experimental measurement in order to demonstrate the feasibility of the identification process. The second was the quantifying of the identification error for the Neo-H parameters. This numerical example was developed as realistic as possible in order to provide an estimation of the identification accuracy.

#### **2.4.1. Development of a numerical example**

The displacement fields corresponding to simulated measurements were built from the finite element model (Fig. 1.B) where the Neo-Hookean parameters ( $C_{10}$ ,  $D$ ) of each material (adipose tissue, quadriceps, ischios, gracilis and sartorius) were fixed according to the

literature and summarized in Table 1. Indeed, in the literature, the muscles of interest (quadriceps, ischios, gracilis and sartorius) were mainly *in vivo* characterized in term of linear elasticity, where the Poisson ration is chosen close to 0.5. Thus, the  $C_{10}$  parameters for the adipose and thigh muscles were calculated from the shear modulus values obtained from *in vivo* MRE (Magnetic Resonance Elastography) measurements [7, 8]. Indeed, assuming the isotropy and the infinitesimal strain theory, the  $C_{10}$  Neo-Hookean parameter was related to the shear modulus ( $\mu$ ) as:  $C_{10} = \mu/2$ . The fixed  $C_{10}$  parameters being in the same range as Tran's study [15], it was decided to fix the D parameters also in the same range from this study.

Subsequently, a finite element simulation was performed with the fixed parameters providing the nodal displacements, which were projected onto a regular data grid revealing the DIC information. The projection was performed with a 16 pixels meshsize corresponding to 64x64 data points. In addition, a Gaussian white noise ( $\delta \sim N(0, \sigma^2)$ ) was added to simulate the experimental noise.

#### 2.4.2. Quantification of the identification error

The identification error was quantified for all the Neo-Hookean parameters as the relative error corresponding to the difference between the reference ( $\theta_{k\_reference}$ ), which was composed of the initial values fixed in the numerical example from the literature (Table 1), and the identified ( $\theta_{k\_identified}$ ) parameter resulting from the identification:

$$Error = \left| \frac{\theta_{k\_identified} - \theta_{k\_reference}}{\theta_{k\_reference}} \right| \quad (4)$$

Five initializations, based on a Latin hypercube, were performed and only the error related to the lowest cost function was presented.

Moreover, in this study, the D parameters of the gracilis, sartorius and ischios muscles, which have similar morphological and functional properties, were grouped in order to decrease the identification error.

### 3. RESULTS

#### 3.1. Optimization of the ultrasound parameters

##### 3.1.1. Frequency

The high frequencies, 13 MHz and 11 MHz, did not provide enough tissue information in depth close to the bone tissue (Figs. 4.B,C). However, Fig. 4.A showed more visible tissue structure in depth using a 9 MHz frequency. Therefore, the DIC was performed on ultrasound images acquired at 9MHz.

##### 3.1.2. Result of the optimal gain for a fixed dynamic

Fig. 6 showed the results of the tested gain for each dynamic. The selected couples (gain, dynamic) were represented by a black circle. It can be noticed the optimal gains, based on the grey level histogram, increased as a function of the dynamic. For the 54 dB and 57 dB dynamics several gains were optimal.

##### 3.1.3. Comparison of the optimal couples

The histogram of the standard deviation for each optimal couples was represented Fig. 7. No significant difference was found between the standard deviations for both horizontal and vertical displacement fields. As a consequence, the random errors were in the same range whatever the couple was. The couple (Dyn: 42 dB, G: 34 dB) was chosen as optimal due to its lower standard deviations for both displacement fields and also for its lower variance (Fig. 7). For the numerical example, the standard deviation of the white noise ( $\delta \sim N(0, \sigma^2)$ ) was chosen equal to 1.5 pixels, corresponding to  $1.76 \cdot 10^{-2}$  mm, for both displacement fields. The noise value was set up according to the standard deviation calculated for the optimal couple (horizontal displacement field: from 0.96 to 1.48 pixels, vertical displacement field: from 0.73 to 1.19 pixels).

### 3.2. Result of the sensitivity analysis

Fig. 8 illustrated the displacement sensitivity for the Neo-Hookean parameters ( $C_{10}$ ,  $D$ ) for the quadriceps muscle as a function of the three different loadings.

The contention test showed a cartography of sensitivity with higher values for the  $D$  parameter (Fig. 8.D) compared to the  $C_{10}$  coefficient (Fig. 8.A). Furthermore, it was observed that the  $D$  parameter had a higher sensitivity within the corresponding muscle (quadriceps) area, while the  $C_{10}$  parameter showed sensitivity randomly localized within the thigh.

The comparison of the Neo-Hookean parameters, obtained with the indentation test, revealed higher sensitivity values for the  $C_{10}$  (Fig. 8.B) compared to the  $D$  coefficient (Fig. 8.E). The high sensitivity values of the  $C_{10}$  parameter were localized in small quadriceps areas. The main drawback of this present test would be the numerous performed indentations, and therefore the corresponding finite element simulations, around the thigh.

Concerning the compression test, the  $C_{10}$  parameter (Fig. 8.C) showed higher sensitivity values than the  $D$  parameters. In addition, the cartography corresponding to the  $D$  coefficient revealed a higher sensitivity in the investigated muscle (quadriceps) (Fig. 8.F).

Similar results were obtained for the other parameters with the three configurations, but not presented, because the results were similar.

The comparison of all the results showed that, for each loading, only one Neo-Hookean parameter ( $C_{10}$  or  $D$ ) had a high sensitivity. It is well known that a high sensitivity value will provide a better identification. In the literature, few studies considered an incompressible Neo-Hookean law (without  $D$ ) for the soft tissues, hence emphasizing the role of  $C_{10}$ . As a consequence, the identification of the  $C_{10}$  parameter was highlighted using the compression test.

### **3.3.Result of the Neo-Hookean parameters**

#### **3.3.1. Identification of the mechanical parameters for each individual tissue**

Figs. 9.A-B showed the results of the  $C_{10}$  and D identification errors for each tissue. These identification errors were obtained from the numerical example with and without experimental noise (0.2mm).

The result of the identified parameters ( $C_{10}$ , D) obtained without noise revealed a low identification error (< 2%) leading to the validation of the developed inverse approach and the use of the BFGS algorithm.

In the presence of the experimental noise, the error on the identification increased for both parameters ( $C_{10}$ , D). A slight increase of the error (<5 %) was found for all the  $C_{10}$  coefficients compared to the high increase of the D parameters error (from 7.5 to 37%). These results demonstrated an accurate identification of the  $C_{10}$  parameters whatever the noise was. However, the identified D parameters required some adjustments, especially for the ischios, sartorius and gracilis muscles. These results are consistent with the sensitivity analysis.

#### **3.3.2. Decrease of the identification error**

To improve the accuracy of the identified D parameters, the compressibility parameters of three muscles (ischios, sartorius and gracilis) were grouped. Thus, Figs. 9.C,D showed the new identification errors obtained for each Neo-Hookean parameter.

Fig. 9.C showed that the grouping of the muscle tissues provided a decrease of the  $C_{10}$  identification error (<3%) with an experimental noise.

Fig. 9.D showed the identification error obtained for the three D parameters composed of the quadriceps, adipose tissue and the group of muscle (ischios, sartorius and gracilis). A decrease of the identified D parameters error (<7%) was found for a typical experimental noise (0.2mm).

## **4. DISCUSSION**

The muscle tissue is a complex system to analyze due to its composition, the inter-individual variability, its temporal evolution and its interactions with other media.

The development of new imaging technology provided a more accurate characterization of the structural properties of the muscle. However, the study of the muscle mechanical behavior still remained a large domain of investigation, too often neglected in various scientific and medical fields. For instance, in the medical field, palpation reflected by the muscle elasticity is often used to detect muscle tension which can be pathological. These data were mainly subjective and there is a real need for clinicians to objectively quantify the severity of a disease or the effect of treatment. The functional properties of the muscle were also important in car crash where muscle tissue is too often neglected in numerical studies. Indeed, the simulation of the muscle behavior is essential because it create an envelope around the skeleton limiting the damages, maintaining the body, and absorbing the shock.

### **4.1.Measured displacement field**

The originality of this present study was to perform the DIC on *in vivo* ultrasound images which was usually used for non biological materials (composite, etc...) [23-26]. The main advantage of this procedure was to use regular ultrasound machine available in clinic and providing anatomical images. Conversely, Zhu's study [19] measured a displacement field from signal and requested the use of an open ultrasound machine, more available in research department. However, the challenge of this developed procedure was to obtain a speckle on the ultrasound images enabling to perform the DIC. Thus, other studies [2-3, 15] avoid the displacement field measurements using anatomical markers (contours of muscle, skin and bone) to build the cost function. Consequently, only few points can be analyzed and

therefore did not provide a local muscle behavior and a less accurate sensitivity of the material parameters.

The comparison of the standard deviation for the horizontal and vertical displacements showed a higher uncertainty for the horizontal one. This result may be due to the propagation of the beam which is parallel to the direction of the loading and close to the natural structure of the muscle tissues. This finding was in agreement with the literature [17] leading the authors to use a cost function only based on the displacement parallel to the beam. In addition, the high standard deviation for both displacement fields could be induced by the muscle movements, such as involuntary contraction or blood flow, providing changes (muscular shift) during the ultrasound acquisitions.

#### **4.2. Constitutive muscle behavior**

Muscle tissue was often considered as linear, elastic and incompressible leading to a Poisson's ratio close to 0.5 [6-7, 9]. Other studies identified the muscle as hyperelastic using Rivlin or Ogden models which include different assumptions [10-14]. In this present study, an hyperelastic model, quite simple, was chosen in order to characterize the nonlinear muscle behavior. The choice was justified since it is a preliminary study where the goal is to demonstrate a novel coupling between FE simulation and DIC based on US imaging, leading to the identification of the mechanical properties of different thigh muscles. Moreover, the choice of a hyperelastic model for *in vivo* characterization was not so frequent step forward, compared to the usual linear elasticity identification performed with US imaging. In addition, a Neo-Hookean behavior was selected due to the unique applied loading and the low induced strain, similarly to the literature [2-3, 15]. In perspective, a more accurate hyperelastic model could be developed using different muscle loadings.

### **4.3.Assumptions of the FE modeling**

The present boundaries between materials were considered perfectly tied as other studies [2-3, 15]. A way to improve the FE modeling would be to add some sliding and friction occurring between each soft tissue [2-3, 15]. In addition, the sliding between the plates, modeled as a rigid body, and the skin was assumed frictionless. The plane strain was used for the present FE modeling avoiding the out of plane displacements. A way to improve this 2D simulation would be to perform a 3D model.

### **4.4.Identification process**

The cost function used for the identification of the muscle mechanical parameters was based on the displacement as Avril's study [2-3, 15]. A way to improve the present cost function would be to include additional terms relative to the loading (force) [15]. Furthermore, a regularization term [16] could be added to drive the solution.

### **4.5.Sensitivity analysis**

The result of the sensitivity analysis showed that both contention and compression tests would be necessary to properly identify the  $C_{10}$  and  $D$  parameters. However, the development and the design of set ups, and the number of finite element simulations, would have increased the computational time, the complexity of the model and the number of experimental tests. One of the originality of this study was to realize a sensitivity analysis revealing the feasibility to identify each Neo-Hookean parameter. Tran and Avril's studies respectively performed indentation and contention tests on muscle (arm and calf) and found different ranges of values for the Neo-Hookean muscle parameters. This could be due to a better identification of one parameter and a sensitivity analysis could have confirmed this assumption.

#### **4.6.Numerical example**

Similarly to the developed numerical example, Gokhale et al. [16] showed also the feasibility to identify the heterogeneous, hyperelastic and compressible properties of soft tissues. Both studies applied the same level of noise (from 0 to 3%) and equivalent results were obtained. Indeed, with and without noise the identification error for each mechanical parameter is low. Moreover, the present results of the identification error were in agreement with the sensitivity analysis. As expected a lower identification error was obtained for the  $C_{10}$  parameters. The perspective of this work would be to replace the numerical example by experimental measurement.

#### **4 CONCLUSION**

The originality of this study was to develop an inverse method, coupling imaging techniques (Ultrasound, MRI) with numerical methods (DIC, FEMU), to identify the muscle mechanical behavior. This novel methodology could have an impact in the scientific and medical fields. Indeed, clinicians are assisted by robotic devices to ensure safe and accurate medical procedures, and these devices require knowledge of the mechanical properties of the muscle (tissue contact). Moreover, in car crash soft tissues are often neglected during the FE simulations while they have an important role in posture and in shock absorption.

#### **CONFLICT OF INTEREST STATEMENT**

All authors do not have conflict of interest.

#### **ACKNOWLEDGEMENT**

This project is co-financed by the European Union engaged in Picardy with the European Regional Development Fund.

## REFERENCES

1. Bringard, R. Denis, N. Belluye, and S. Perrey. Compression élastique externe et fonction musculaire chez l'homme, *Science & sports*, 22(1): 3-13, 2007
2. S. Avril, P. Badel, L. Dubuis, P.Y. Rohan, J. Debayle, S. Couzan, and J.F. Pouget. Patient-Specific Modeling of Leg Compression in the Treatment of Venous Deficiency, *Patient-Specific Modeling in Tomorrow's Medicine*, 217-238, 2012
3. S. Avril, L. Bouten, L. Dubuis, S. Drapier, and J.F. Pouget. Mixed experimental and numerical approach for characterizing the biomechanical response of the human leg under elastic compression, *Journal of biomechanical engineering*, 132: 31006-31014, 2010
4. L. Dubuis, S. Avril, J. Debayle and P. Badel. Identification of the material parameters of soft tissues in the compressed leg. *Computer Methods in Biomechanics and Biomedical Engineering*, 15: 3–11, 2012
5. J. Bercoff, M. Tanter, and M. Fink. Supersonic shear imaging: a new technique for soft tissue elasticity mapping. *Ultrasonics, Ferroelectrics and Frequency Control, IEEE Transactions on*, 51(4): 396-409, 2004
6. J.L. Gennisson, T. Deffieux, E. Macé, G. Montaldo, M. Fink and M. Tanter. Viscoelastic and anisotropic mechanical properties of in vivo muscle tissue assessed by supersonic shear imaging, *Ultrasound in medicine & biology*, 36(5): 789-801, 2010
7. S.F. Bensamoun, S.I. Ringleb, L. Littrell, Q. Chen, M. Brennan, R.L. Ehman and K.N. An. Determination of thigh muscle stiffness using magnetic resonance elastography, *Journal of Magnetic Resonance Imaging*, 23(2): 242-247, 2006
8. G.E. Leclerc, F. Charleux, L. Robert, M.C. Ho-Ba-Tho, C. Rhein, J.P. Latrive and S.F. Bensamoun. Analysis of liver viscosity behavior as a function of multifrequency

- magnetic resonance elastography (MMRE) postprocessing, *Journal of Magnetic Resonance Imaging*, 38(2): 952-957, 2013
9. L. Debernard, G.E. Leclerc, L. Robert, F. Charleux and S.F. Bensamoun. In vivo characterization of the muscle viscoelasticity in passive and active conditions using multifrequency MR Elastography. *Journal of Musculoskeletal Research*, 16(2): 397-401, 2013
  10. E. Linder-Ganz, N. Shabshin, Y. Itzhak and A. Gefen. Assessment of mechanical conditions in sub-dermal tissues during sitting: a combined experimental-MRI and finite element approach, *Journal of biomechanics*, 40(7): 1443-1454, 2007
  11. C. Then. T.J. Vogl and G. Silber. Method for characterizing viscoelasticity of human gluteal tissue, *Journal of biomechanics*, 45(7): 1252-1258, 2012
  12. T.J. Vogl, C. Then, N.N. Naguib, N.E.A. Nour-Eldin, M. Larson, S. Zangos and G. Silber. Mechanical Soft Tissue Property Validation in Tissue Engineering Using Magnetic Resonance Imaging: Experimental Research, *Academic radiology*, 17(12): 1486-1491, 2010
  13. F.M. Hendriks, D. Brokken, C.W.J. Oomens, D.L. Bader and F.P.T. Baaijens. The relative contributions of different skin layers to the mechanical behavior of human skin in vivo using suction experiments, *Medical Engineering & Physics*, 28(3): 259-266, 2006
  14. F.M. Hendriks, D. Brokken, J. Van Eemeren, C.W.J. Oomens, F.P.T. Baaijens and J. Horsten. A numerical-experimental method to characterize the non-linear mechanical behaviour of human skin, *Skin Research and Technology*, 9(3): 274-283, 2003
  15. H.V. Tran, F. Charleux, M. Rachik, A. Ehrlacher and M.C. Ho-Ba-Tho. In vivo characterization of the mechanical properties of human skin derived from MRI and

- indentation techniques, *Computer Methods in Biomechanics and Biomedical Engineering*, 10(6): 401-407, 2007
16. N.H. Gokhale, P.E. Barbone and A.A. Oberai. Solution of the nonlinear elasticity imaging problem: the compressible case, *Inverse Problems*, 24(4): 045010, 2008
  17. A.A. Oberai, N.H. Gokhale, S. Goenezen, P.E. Barbone, T.J. Hall, A.M. Sommer and J. Jiang. Linear and nonlinear elasticity imaging of soft tissue in vivo: demonstration of feasibility, *Phys. Med. Biol.*, 54: 1191-1207, 2009
  18. T.J. Hall, P.E. Barbone, A.A. Oberai, J. Jiang, J.F. Dord, S. Goenezen and T.G. Fisher. Recent results in nonlinear strain and modulus imaging, *Curr Med Imaging rev*, 7(4): 313-327, 2011
  19. Y. Zhu and T.J. Hall. A modified block matching method for real-time freehand strain imaging, *Ultrasound. Imaging*, 24(3): 161-176, 2002
  20. Y. Fu, C. Chui, C. Teo and E. Kobayashi. Motion tracking and strain map computation for quasi-static magnetic resonance elastography, *Medical Image Computing and Computer-Assisted Interventional MICCAI 2011*, 428-435, 2011
  21. K.M. Moerman, A.M.J. Sprengers, A.K. Nederveen and C.K. Simms. A novel MRI compatible soft tissue indenter and fibre Bragg grating force sensor, *Medical Engineering & Physics*, 35(4): 486-499, 2012
  22. J.S. Affagard, P. Feissel, S.F. Bensamoun. Measurement of the quadriceps muscles displacement and strain fields with ultrasound and Digital Image Correlation (DIC) techniques, *IEEE Trans. Biomed. Eng.*, *in press*
  23. F. Hild and S. Roux. Digital image correlation: from displacement measurement to identification of elastic properties - a review, *Strain*, 42(2): 69-80, 2006
  24. F. Hild and S. Roux. CorreliQ4: A software for finite element displacement field measurements by digital image correlation, *Internal report (269)*, 2008

25. L. Chevalier, S. Calloch, F. Hild and Y. Marco. Digital image correlation used to analyze the multiaxial behavior of rubber-like materials, *European Journal of Mechanics-A/Solids*, 20(2): 169-187, 2005
26. M. Grediac and F. Hild. *Mesures de champs et identification en mécanique des solides (Série matériaux et métallurgie, MIM)*, Lavoisier, 2011
27. Abaqus/6.9, 2009, 6.9 Software, User's Manual (6.9), Inc. and Dassault Systemes
28. Scan IP. <http://www.simpleware.co.uk>, 2010.
29. Tarantola. *Inverse problem theory*, Elsevier Amsterdam etc, 1987
30. J.S. Affagard, S.F. Bensamoun, P.Feissel. Inverse method to identify the muscle mechanical properties, *Euromech colloquium 534, Advanced experimental approaches and inverse problems in tissue biomechanics*, 2012

*Table 1: Summary of the fixed parameters ( $C_{10}$ ,  $D$ ) calculated from the literature*

Soft tissues	fat		Ischio		quadiceps		Gracilis		Sartorius	
Neo-Hookean ( $C_{10}$ : kPa, $D$ : MPa-1)	$C_{10}^f$	$D^f$	$C_{10}^i$	$D^i$	$C_{10}^q$	$D^q$	$C_{10}^g$	$D^g$	$C_{10}^s$	$D^s$
Chosen parameters	0.8	30.8	3	18	1.75	18	2.2	18	3.75	18

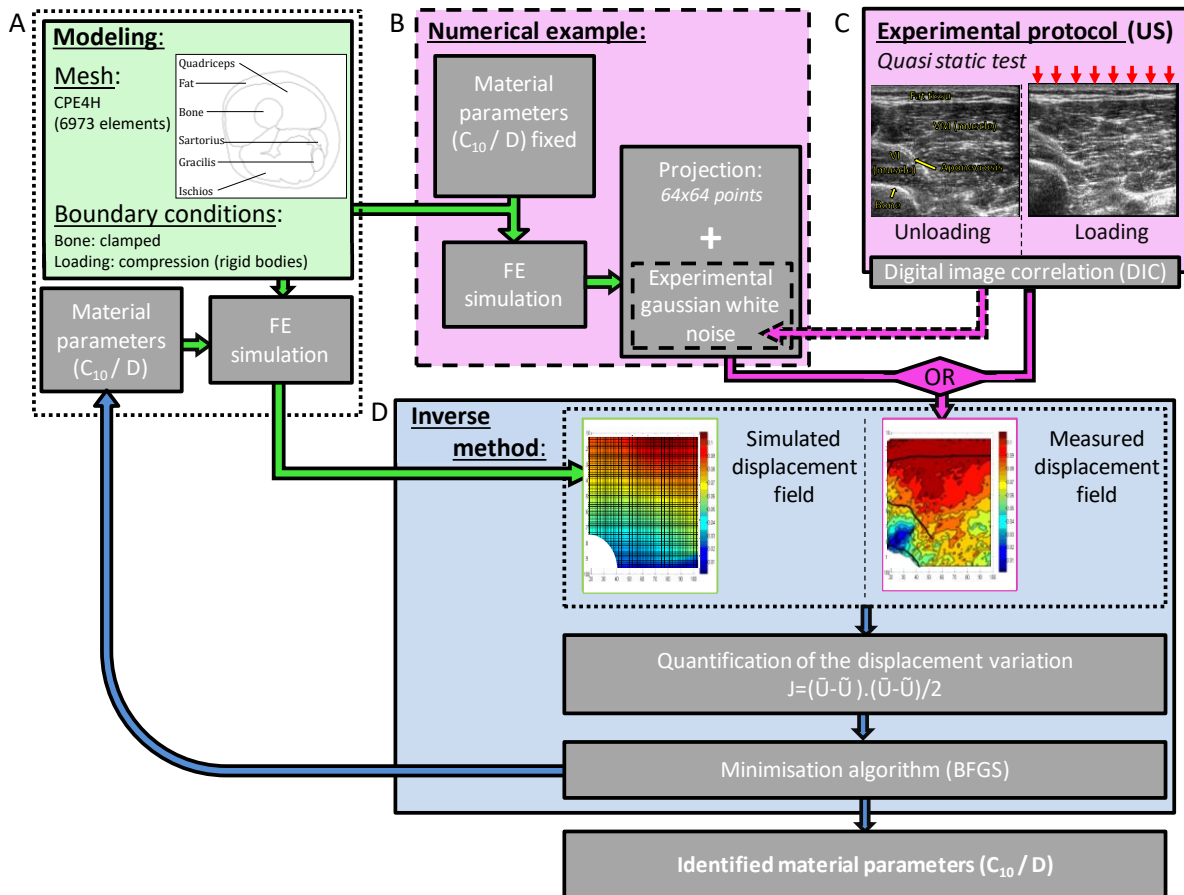


Figure 1: Finite Element Model Upgrading (FEMU) composed of (A) Mechanical modeling, (B) Numerical example, (C) Experimental protocol, and (D) inverse method.

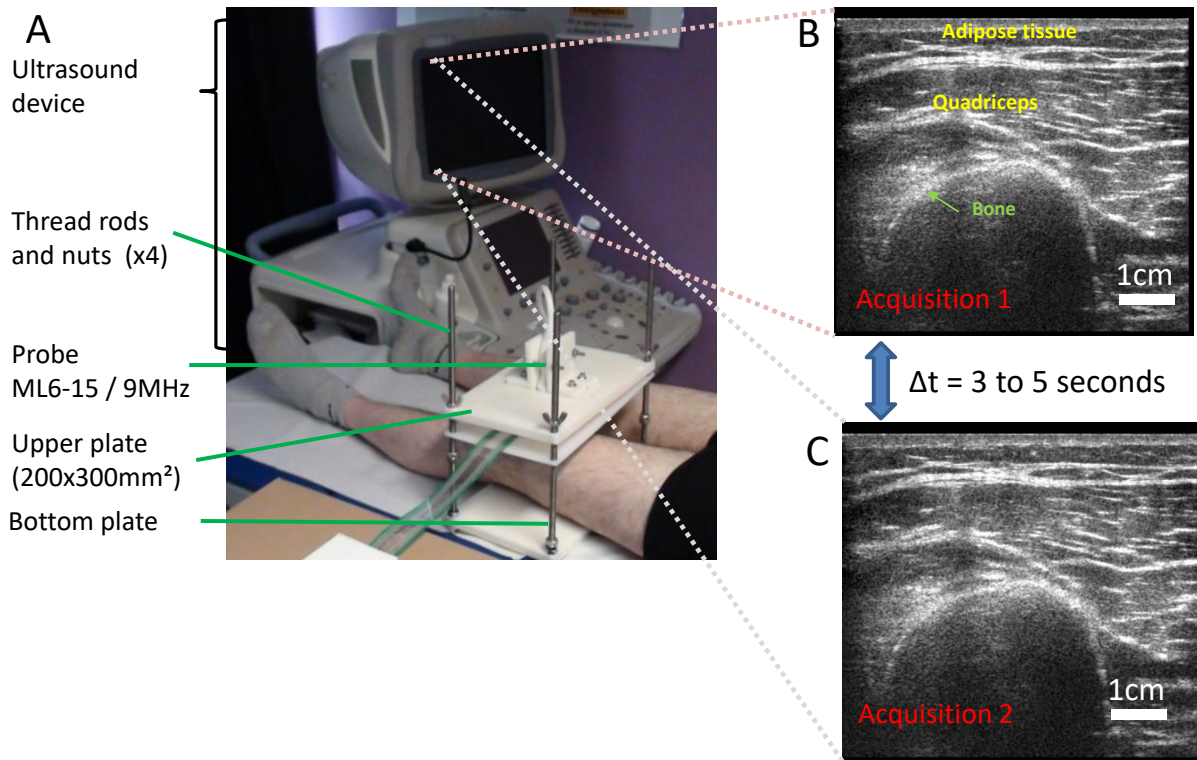


Figure 2: (A) Experimental protocol used for the acquisitions of the successive ultrasound image performed without loading (B-C). The DIC was applied on these images.

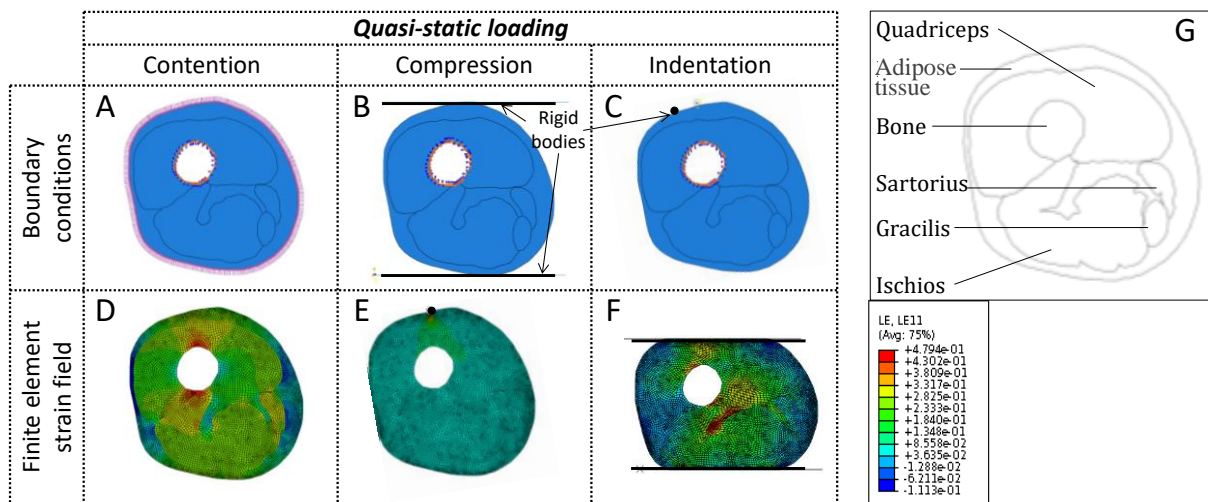


Figure 3: Simulation of the different static tests: (A) contention, (B) indentation and (C) compression and (D-E-F) their engineering strain following the direction 1 (LE11) on the deformed shape. (G) Geometry of the thigh use for the finite element simulation

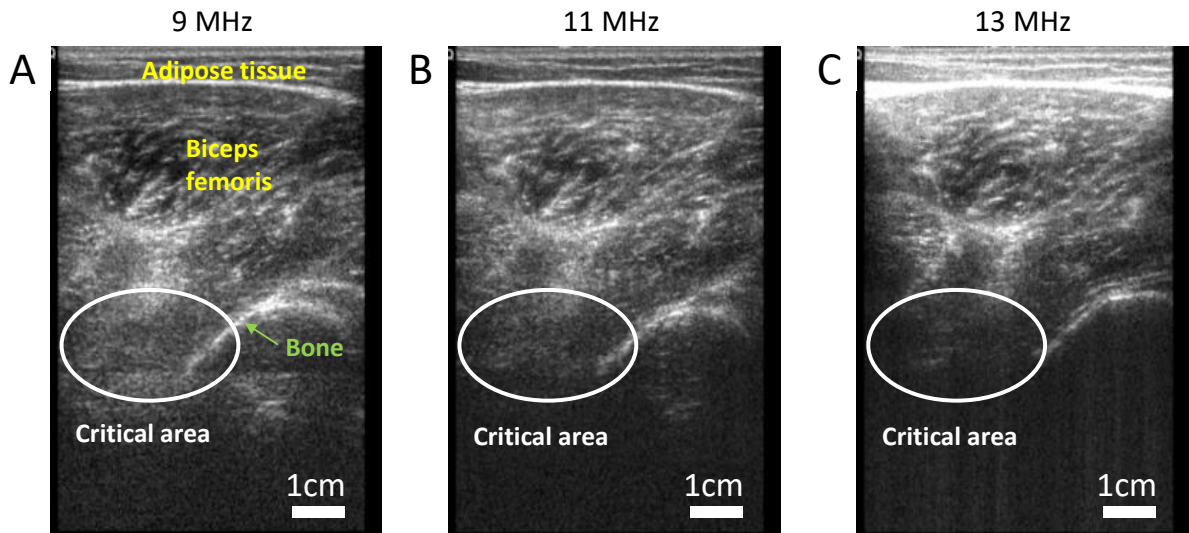


Figure 4: Ultrasound image obtained with a frequency of 9MHz (A), 11MHz (B) and 13MHz (C)

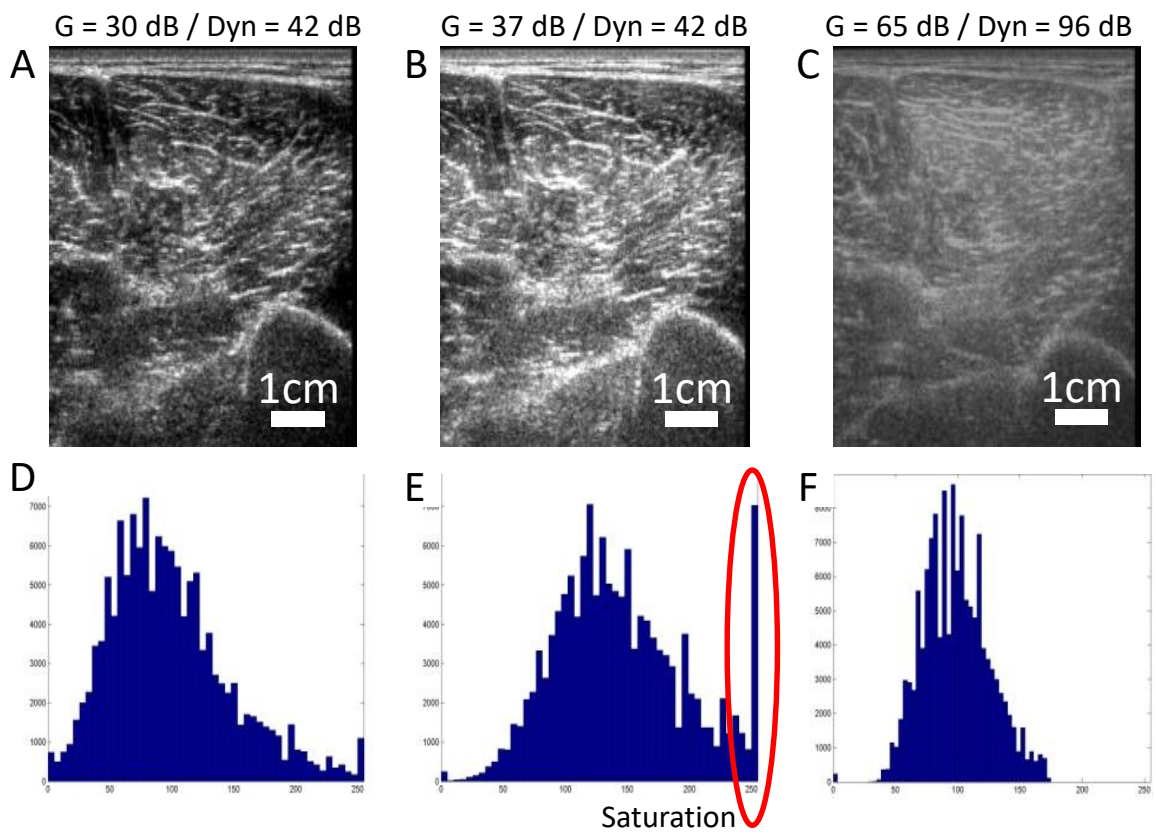


Figure 5: Grey level histograms corresponding to the ultrasound images for three different couples (G: gain / Dyn: dynamic).

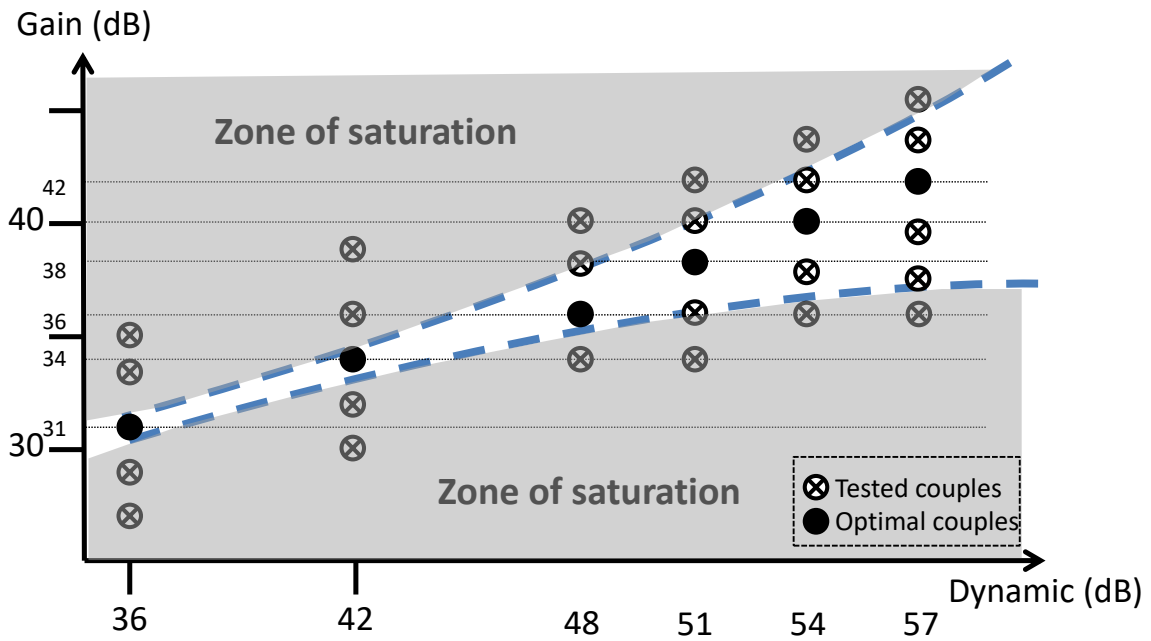


Figure 6: Selection of the optimal gain at a fixed dynamic based on the result of the grey level histogram obtained at 9 MHz.

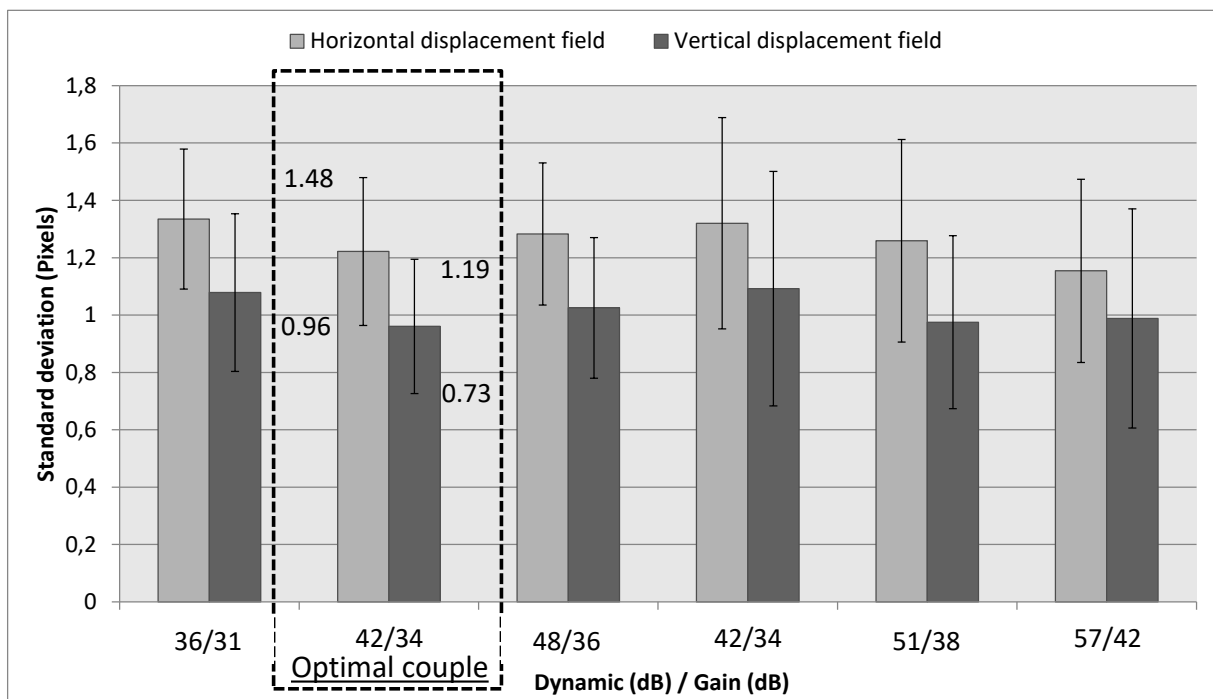


Figure 7: Standard deviation of the horizontal and vertical displacement fields for a 8 pixels meshsize as a function of the optimal couples

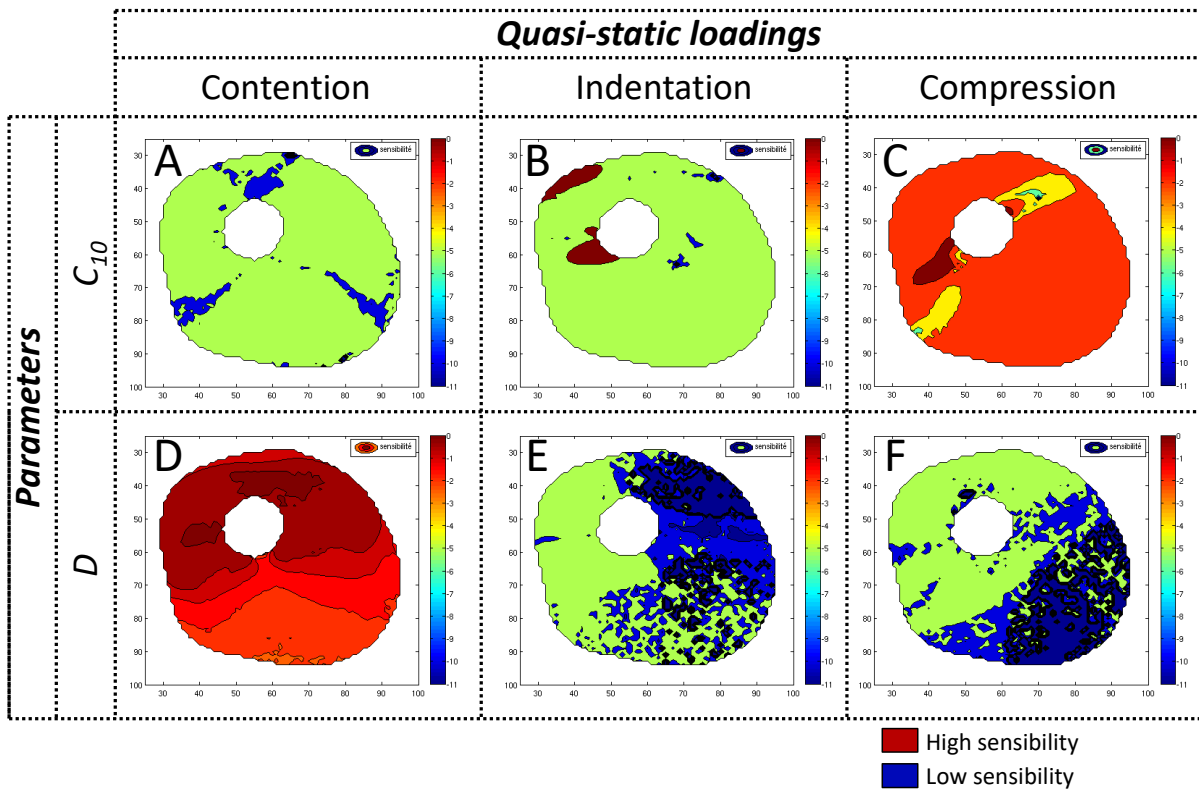
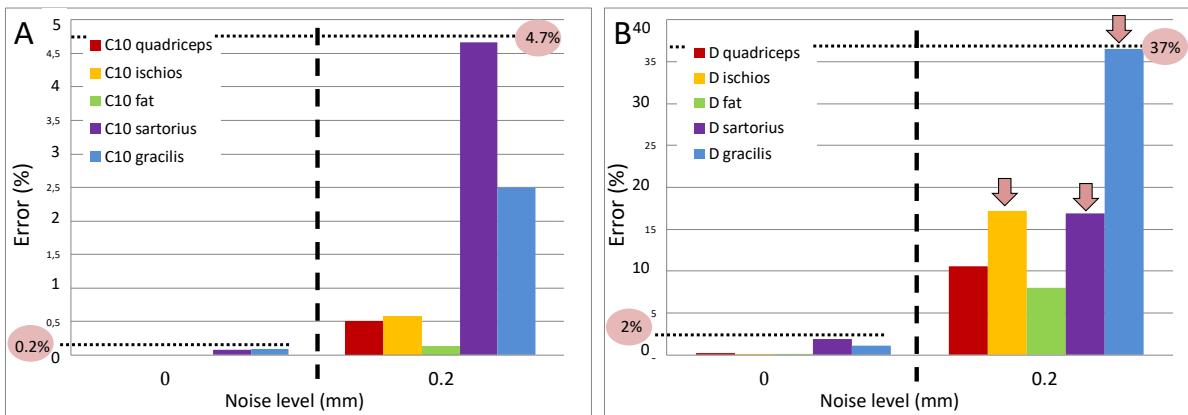


Figure 8: Cartographies of the displacement sensitivity for the Neo-Hookean parameters of the quadriceps muscle following the contention (A-D), the indentation (B-E) test and the compression (C-F) loading.

### Identification errors for each tissue



### Identification errors for each tissue with grouped muscle assumption

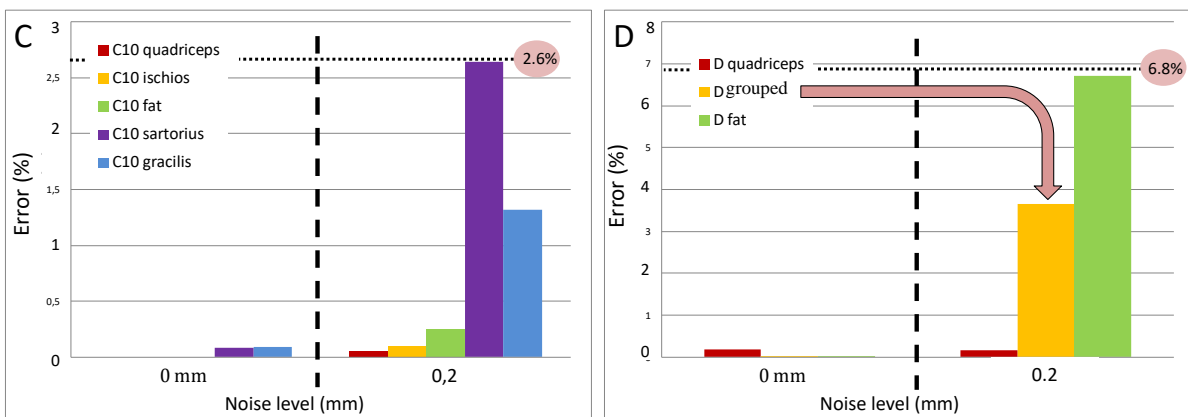


Figure 9: Identification of the relative error obtained for the  $C_{10}$  and  $D$  parameters without (A) and with noise (B). Arrows located on figure B indicate the high percentage of error obtained for the  $D$  parameters and the arrow figure D showed the decrease of the error when the muscles (ischios, gracilis, Sartorius) are grouped (C-D).